Dynamic of Passive Guidance Forces of Polarized Linear Motors Application to Swissmetro MAGLEV

Alain CASSAT[1)], Christophe ESPANET[2)], Vincent BOURQUIN[3)], Yves PERRIARD[1)]
[1)]Ecole Polytechnique Fédérale de Lausanne, EPFL-STI-IPR-LAI, CH-1015 Lausanne, Switzerland
Tel: +41(0)21 693 26 91 – Fax: +41(0)21 693 26 87 – e-mail: alain.cassat@epfl.ch
[2)]University of Franche-Comté, Laboratory of Research in Electrical Engineering and Systems
Tel: +33(0)3 845 8 3614 – Fax: +33(0)3 845 8 3636 – e-mail: christophe.espanet@univ-fcomte.fr
[3)]Numexia, EPFL-PSE-A, CH-1015 Lausanne, Switzerland
Tel: +41(0)21 693 87 37 – e-mail: vincent.bourquin@numexia.com

1. Introduction

Maglev (>400 km/h) refer to Maglev [1] such as the Japanese JR-Maglev MLX, the German Transrapid and the USA Inductrack. The Swissmetro Project, presenting a unique aspect of Maglev, is designed to work under partial vacuum (<10 kPa) in two tunnels. The authors investigate the combination of the propulsion with the levitation (Figure 1). To minimize the heat due to the iron and copper losses, a polarized excitation is proposed [2] with NdFeB PM for the magnetic way poles. The papers [3, 4] present the determination of the static guidance forces, produced by the magnetic way, and a first order analysis of the corresponding lateral dynamic behavior.

This paper emphasis the dynamic of the vehicle guidance due to these passive guidance forces interacting with the real profile of the long stator track. The main goal is to determine: *if the iron losses created in the magnetic way (PM and poles) can produce enough dynamic damping for the lateral passive guidance*.

Conventional 3D FEM software does not permit to determine the iron losses of a magnetic system having simultaneously two movements in two orthogonal axes (propulsion O_x, lateral guidance O_z). *As a first investigation, a quasi stationary approach is proposed based on 3D FEM analysis of the magnetic system*. For a constant vehicle speed, the iron losses of the magnetic way are determined as a function of the lateral eccentricity. Then the lateral effect is assumed in *a quasi stationary behavior*, considering the real track profile. The issues related to such an approach, are described.

2. Main Guidance Specifications

All specifications are given in [3, 4, 5]. Two cases are considered for the vehicle guidance.

Specification 1 - passenger comfort: for an acceleration of 0.8 [m/s^2], a vehicle mass of 80 [tons] and a non total compensation of the acceleration, the necessary guidance force is equal to 64 [kN].

$$F_{guidance} = m_{vehicle} \cdot a_{comfort} = 64000 \quad [N] \quad (1)$$

Specification 2 - vehicle at stalls: when the vehicle stalls, in a curve of 9.66° inclination, the force becomes:

$$F_{guidance} = m_{vehicle} \cdot g \cdot \sin(\alpha) = 134240 \quad [N] \quad (2)$$

3. Passive Guidance Forces

The passive guidance forces [5] are produced by the reluctant effect between the long stator and the magnetic way. To study the guidance specifications, 3D FEM analysis are carried out. Figure 3 shows a static 3D model with both longitudinal and transverse views of the motor. This elementary model is used to compute the passive guidance forces. Figure 4 presents the dynamic case corresponding to a partial magnetic way, having a transverse eccentricity Z_z, composed of two poles moving at the vehicle speed.

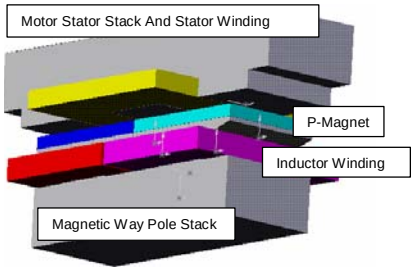

Figure 1: Motor: combined propulsion with levitation, two magnetic poles and three stator teeth are presented.

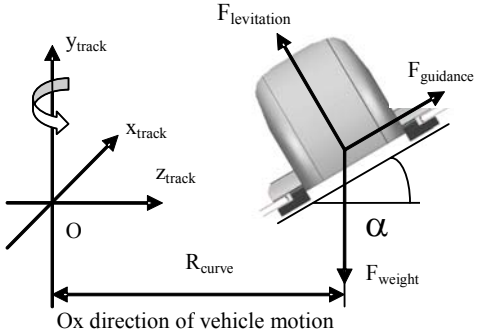

Figure 2: Vehicle in a curve: inclination α, radius R_{curve}.

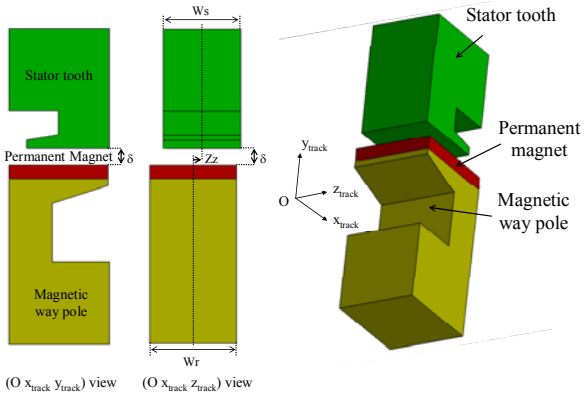

Figure 3: Motor – 3D FEM model.

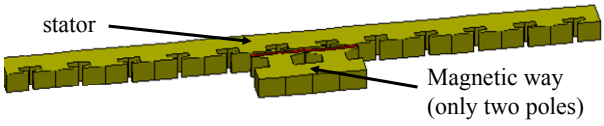

Figure 4: 3D FEM model for the iron loss determination.

4. Damping Effects

4.1. Approach

To evaluate the damping effects, both magnetic and mechanical studies are considered. A FEM strategy is proposed and a simplified mechanical system is defined.

4.2. FEM Strategy

3D FEM software does not permit to determine the iron losses of a magnetic system having *simultaneously two movements in two orthogonal axes*. The following developments suggest a FEM strategy.

In dynamic, the passive guidance forces comprise a damping effect produced mainly by the permanent magnet iron losses, since the magnetic way has laminated yokes and poles. These losses are produced by the slot effect of the stator in the direction of the vehicle motion and by the variation of the transverse eccentricity (reluctant effect) due to the real track profile.

In a first mathematical understanding, it can be assumed that the PM losses are proportional to the power two of the temporal derivative of the PM magnetic flux, in other words, the back EMF produced in the PM. This means that, in a first order analysis, the "global" PM resistance does not vary versus the spatial position (small variation of the transverse eccentricity). For time t, once the system is determined, it can be linearized around the spatial positions (x, y, z). Then the total flux, crossing one magnetic pole and more particularly one PM pole, and its total derivative become:

$$\Psi_{PM} = \Psi_{PM}(x, y, z) \qquad [Vs] \quad (3)$$

$$d\Psi_{PM} = \frac{\partial \Psi_{PM}}{\partial x} \cdot dx + \frac{\partial \Psi_{PM}}{\partial y} \cdot dy + \frac{\partial \Psi_{PM}}{\partial z} \cdot dz \quad [Vs] \quad (4)$$

Then the corresponding back EMF is expressed as follows, for a constant air gap ($y_s = y_{wr} = y_{wl} = \delta$) of the magnetic way:

$$\frac{d\Psi_{PM}}{dt} = \frac{\partial \Psi_{PM}}{\partial x} \cdot \dot{x} + \frac{\partial \Psi_{PM}}{\partial z} \cdot \dot{z} \qquad [V] \quad (5)$$

And the power two of the back EMF becomes:

$$\left(\frac{d\Psi_{PM}}{dt}\right)^2 = \left(\frac{\partial \Psi_{PM}}{\partial x} \cdot \dot{x}\right)^2 + 2 \cdot \frac{\partial \Psi_{PM}}{\partial x} \cdot \dot{x} \cdot \frac{\partial \Psi_{PM}}{\partial z} \cdot \dot{z} + \left(\frac{\partial \Psi_{PM}}{\partial z} \cdot \dot{z}\right)^2 \qquad [V^2] \quad (6)$$

Admitting that the "global" PM resistance does not vary, the previous equation suggests, that the damping force produced by the PM losses is proportional to the following terms representing a magnetic drag force:

$$F_{PMx} \approx k \cdot \left(\frac{\partial \Psi_{PM}}{\partial x}\right)^2 \cdot \dot{x} \qquad [N] \quad (7)$$

$$F_{PMz} \approx k \cdot \left(\frac{\partial \Psi_{PM}}{\partial z}\right)^2 \cdot \dot{z} \qquad [N] \quad (8)$$

The factor k is homogeneous to an electrical resistance. Equation 6 becomes, considering Equations 7 and 8:

$$k \cdot \left(\frac{d\Psi_{PM}}{dt}\right)^2 \approx F_{PMx} \cdot \dot{x} + 2 \cdot \sqrt{F_{PMx} \cdot F_{PMz} \cdot \dot{x} \cdot \dot{z}} + F_{PMz} \cdot \dot{z} \qquad [V^2] \quad (9)$$

Then, per analogy, the resulting damping force in the direction Ox is:

$$Fx_{PM} = F_{PMx} + \sqrt{F_{PMx} \cdot F_{PMz} \cdot \frac{\dot{z}}{\dot{x}}} \qquad [N] \quad (10)$$

Similarly, the resulting damping force in the direction Oz is:

$$Fz_{PM} = F_{PMz} + \sqrt{F_{PMx} \cdot F_{PMz} \cdot \frac{\dot{x}}{\dot{z}}} \qquad [N] \quad (11)$$

With: $F_{PMx} < 0$, $\frac{F_{PMz}}{\dot{z}} < 0$ and $\dot{x} > 0$, due to the physical conditions and phenomena.

Equations 10 and 11 suggest that, investigating the effect of each of the two movements (Ox, Oz directions), then combining those, a first order analysis can be made.

4.3. Mechanical System

Different papers present [6, 7] the concept of the mechanical analysis of Maglev in motion. Here, a simplified mechanical system of the vehicle and the magnetic ways are defined assuming the following:

- the vehicle comprises a primary system composed of the vehicle cell and the key electromechanical components. The corresponding mass is m_{pr};
- a secondary mass is composed, on both side of the vehicle, of the motor magnetic ways and the corresponding electromechanical components. The secondary mass is m_{se}.

Figure 5 represents the mechanical scheme of the vehicle and the different spatial referential. The mass of the vehicle has two components, the primary mass and the secondary mass.

$$m_{vehicle} = m_{pr} + m_{se} \qquad [kg] \quad (12)$$

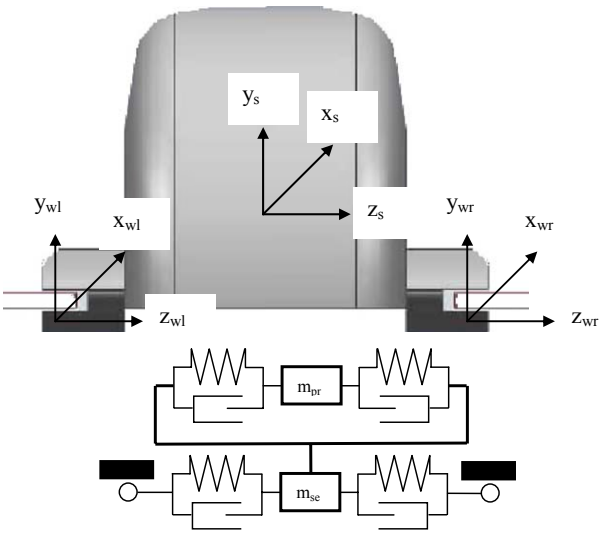

Figure 5: Referential system and mechanical system.

4.4. Dynamic Equations

As a first order analysis of the dynamic behavior, the following assumptions are defined:

- the vehicle primary and secondary systems are rigid in the directions x_s, x_w and y_s, y_w;
- the vehicle speed $v_{vehicle}$ is constant;
- the motor air gap is assumed to be constant: 20±2 [mm].

Defining the referential system of Figure 5, the above

assumptions lead to the following conditions.

$$\left.\begin{aligned} x_s &= x_{wr} = x_{wl} \\ y_s &= y_{wr} = y_{wl} = Y_{vehicle} \\ z_{wr} &= z_{wl} \end{aligned}\right\} \quad [m] \qquad (13)$$

The real track (Fig. 6) has a profile defined in Equation 14.

$$\left.\begin{aligned} x_{tr} &= x_{tl} = v_{vehicle} \cdot t \\ y_{tr} &= y_{tl} = Yt = constant \\ \omega_{track} &= \frac{\pi}{D_{track}} \cdot v_{vehicle} \\ z_{tr} &= d \cdot \sin(\omega_{track} \cdot t) \\ z_{tl} &= d \cdot \sin(\omega_{track} \cdot t + \beta_0) \end{aligned}\right\} \quad [m] \qquad (14)$$

$$\left.\begin{aligned} \dot{x}_{tr} &= \dot{x}_{tl} = v_{vehicle} \\ \dot{y}_{tr} &= \dot{y}_{tl} = 0 \\ \dot{z}_{tr} &= d \cdot \omega_{track} \cdot \cos(\omega_{track} \cdot t) \\ \dot{z}_{tl} &= d \cdot \omega_{track} \cdot \cos(\omega_{track} \cdot t + \beta_0) \end{aligned}\right\} \quad [N] \qquad (15)$$

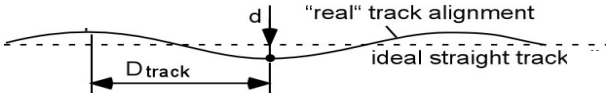

Figure 6: Real track alignment.

As a first order analysis, the passive guidance forces are:

$$\left.\begin{aligned} Fz_{wr} &= kz \cdot (z_{tr} - z_{wr}) + k_{loss_{PM_r}} \cdot \dot{z}_{wr} \\ Fz_{wl} &= kz \cdot (z_{tl} - z_{wl}) + k_{loss_{PM_l}} \cdot \dot{z}_{wl} \\ Fz_w &= Fz_{wr} + Fz_{wl} \end{aligned}\right\} \quad [N] \qquad (16)$$

$$\left.\begin{aligned} x_s &= x_{wr} = x_{wl} = x_{vehicle} \\ \dot{x}_s &= \dot{x}_{wr} = \dot{x}_{wl} = v_{vehicle} \\ \ddot{x}_s &= \ddot{x}_{wr} = \ddot{x}_{wl} = a_{vehicle} \end{aligned}\right\} \qquad (17)$$

For the y coordinate, the air gap δ is assumed constant:

$$\left.\begin{aligned} y_s &= y_{wr} = y_{wl} = \delta \\ \dot{y}_s &= \dot{y}_{wr} = \dot{y}_{wl} = 0 \\ \ddot{y}_s &= \ddot{y}_{wr} = \ddot{y}_{wl} = 0 \end{aligned}\right\} \qquad (18)$$

$$Fy_w = m_{vehicle} \cdot g \cdot \cos(\alpha) \quad [N] \qquad (19)$$

For the z coordinate, the dynamic of the system becomes:

$$\left.\begin{aligned} m_{pr} \cdot \ddot{z}_s &= k_{pr} \cdot (z_s - z_{wr}) - m_{pr} \cdot g \cdot \sin(\alpha) + k_{pr_d} \cdot (\dot{z}_s - \dot{z}_{wr}) \\ m_{se} \cdot \ddot{z}_{wr} &= Fz_w - m_{se} \cdot g \cdot \sin(\alpha) \end{aligned}\right\} \quad [N] \qquad (20)$$

4.5. Damping Effect – Axis Ox

As the vehicle speed is constant, the iron losses have two components, a DC value and an oscillating term, such as, considering only the first harmonic (right track):

$$P_{PMx} = \hat{P}_{PMx} + \Delta\hat{P}_{PMx} \cdot \sin(\omega_{cogging} \cdot t) \quad [W] \qquad (21)$$

$$\hat{P}_{PMx} >> \Delta\hat{P}_{PMx} \quad [W] \qquad (22)$$

The damping force is equal to, for the right track:

$$F_{PMx_r} = \frac{\hat{P}_{PMx_r} + \Delta\hat{P}_{PMx_r} \cdot \sin(\omega_{cogging} \cdot t)}{v_{vehicle}} \quad [N] \qquad (23)$$

The damping factor is equal to:

$$k_{loss_{xr}} = \frac{\hat{P}_{PMx_r} + \Delta\hat{P}_{PMx_r} \cdot \sin(\omega_{cogging} \cdot t)}{v_{vehicle}^2} \quad [Ns/m] \qquad (24)$$

$$k_{loss_{xr}} \approx \frac{\hat{P}_{PMx_r}}{v_{vehicle}^2} \quad [Ns/m] \qquad (25)$$

4.6. Damping Effect – Axis Oz

Considering a simple oscillator permitting to have a first overview of the damping effect, the following developments can be made. When the real track profile is considered (Equations 14), the PM iron losses have a DC value and oscillating terms, such as (right track):

$$\left.\begin{aligned} P_{PMz_r}(t) &= P_{0_{z_r}} + \sum_{\nu=1}^{\nu=\infty} \left[{}^{\nu}P_{1_{z_r}} \cdot \cos(\nu \cdot \omega_{track} \cdot t) + {}^{\nu}P_{2_{z_r}} \cdot \sin(\nu \cdot \omega_{track} \cdot t) \right] \\ P_{0_{z_r}} &= P_{0_{z_r}}(Zz, z_{wr}, \omega_{track}) \\ {}^{\nu}P_{1_{z_r}} &= {}^{\nu}P_{1_{z_r}}(Zz, z_{wr}, \omega_{track}) \\ {}^{\nu}P_{2_{z_r}} &= {}^{\nu}P_{2_{z_r}}(Zz, z_{wr}, \omega_{track}) \end{aligned}\right\} \quad [W] \qquad (26)$$

The damping force and coefficient become (right track):

$$F_{PMz_r}(t) = \frac{P_{PMz_r}(t)}{\dot{z}_{tr}} = \frac{P_{PMz_r}(t)}{d \cdot \omega_{track} \cdot \cos(\omega_{track} \cdot t)} \quad [N] \qquad (27)$$

$$k_{PMz_r} = \frac{F_{PMz_r}(t)}{d \cdot \omega_{track} \cdot \cos(\omega_{track} \cdot t)} \quad [Ns/m] \qquad (28)$$

The force has the same periodicity than the speed.

4.7. Mutual damping factor

The mutual damping factor (Equ. 10, 11) is defined as:

$$k_{loss_{xz_r}} = F_{PMx} \cdot \frac{\dot{x}}{\dot{z}^2} \quad [Ns/m] \qquad (29)$$

4.8. Damping factor

For the right track the damping factor is defined as:

$$k_{loss_{PM_r}} = k_{loss_{z_r}} + \sqrt{k_{loss_{z_r}} \cdot k_{loss_{xz_r}}} \quad [Ns/m] \qquad (30)$$

4.9. Numerical Values - Axis Ox

Table 1 shows the damping factor $k_{loss_{x_r}}$ as a function of the PM iron losses, in the direction Ox. For Swissmetro, the total mechanical power is 6 [MW], corresponding to 3 [MW] on each vehicle magnetic way (right, left sides).

P_{mec_r}	$\hat{P}_{PMx_r}$	$v_{vehicle}$	F_{PMx_r}	$k_{loss_{x_r}}$
[MW]	[kW]	[m/s]	[N]	[Ns/m]
3	-3.53 (a)	139	-25.4	-0.183
3	-5.30 (b)	139	-38.1	-0.274

Table 1: Damping factor $k_{loss_{x_r}}$ function of the PM losses - (a) 8 PM segments; (b) 4 PM segments

4.10. Numerical Values - Axis Oz

Table 2 gives the forces and the damping coefficients for the chosen track profile, as a function of the PM ${}^{1}\hat{F}_{PMz_r}$, in the axes Oz.

D_{track}	d	$v_{vehicle}$	ω_{track}	$\dot{z}_{max}$
[m]	[mm]	[m/s]	[1/s]	[m/s]
50.4	3.0	139	8.66	0.026

${}^{1}\hat{F}_{PMz_r}$	${}^{1}\hat{k}_{loss_{z_r}}$
[N]	[Ns/m]
-0.1	-7.7
-0.3	-11.6
-0.4	-15.4
-0.5	-19.3

Table 2: Forces ${}^{1}\hat{F}_{PMz_r}$ function of the track profile and damping coefficients ${}^{1}\hat{k}_{loss_{z_r}}$.

5. 3D FEM Simulation Results

5.1. Static 3D FEM Simulations Results

The static simulations were carried out in [5]. Figure 5 gives the spatial distribution of the flux lines around the air-gap in a transverse plane. The passive guidance forces were determined [5] in a permanent behavior (constant vehicle speed and constant transverse eccentricity). Figure 6 represents the passive guidance forces corresponding to this case.

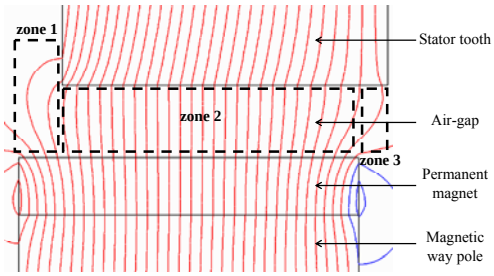

Wr=94 mm; Ws=90 mm; Air gap=20 mm; eccentricity Zz=10 mm

Figure 5: Air-gap flux lines in the transverse plane.

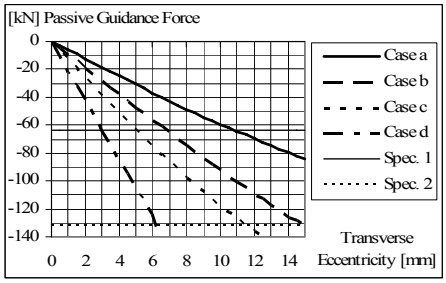

Single magnetic way: *a*: Wr=112 mm; Ws=90 mm; Air gap =20 mm;
c: Wr=112 mm; Ws=90 mm; Air gap =10 mm;
Two magnetic ways: b: Wr=56 mm; Ws=45 mm; Air gap =20 mm;
d: Wr=56 mm; Ws=45 mm; Air gap =10 mm.

Figure 6: Passive guidance force versus transverse offset.

5.2. Dynamic 3D FEM Simulation Results

For the dynamic 3D FEM simulations, only the *case a*, of Figure 6 is considered: Wr=112 [mm]; Ws=90 [mm]; air gap =20 [mm]. Two PM segmentations are investigated: the first one with 4 PM and the second one with 8 PM. Then two types of simulations are carried out. The first simulations deal with longitudinal motions at constant speed of 139 [m/s]. The second ones deal with oscillating transversal motions corresponding to the profile track of Table 2.

In both types of simulations, during the first computation steps, the electrical conductivity is set to a low value in order to reduce the transient time duration due to eddy current establishment. Consequently, during the first steps of the simulations the losses are very low but the results have not to be considered since the conductivity is wrong (Fig. 13). The behaviour of the magnetic materials is assumed to be linear (constant permeability).

In the simple model, only two poles are considered (Fig. 4). For each case, the total PM losses in the whole Swissmetro are computed. For longitudinal simulations, only the case where there is no transverse eccentricity is studied. For transversal simulations, two longitudinal positions of the magnetic way versus the stator are considered. In the first one (axis d), a stator tooth is in the pole transition axis and in the second one (axis q), a stator slot is in the pole transition axis.

Figures 7 and 8 show the spatial repartition of the eddy current density in the permanent magnets, showing that:

- the currents are localized in the each segment;
- the use of 8 PM segments leads to a decrease of the eddy currents density.

Table 3 summarizes the configurations considered for the results given in Figures 9 to 16.

3D FEM simulation cases	Transverse motion, 4 PM, axis d	Transverse motion, 4 PM, axis q	Longitudinal motion, 4 PM	Transverse motion, 8 PM, axis d	Longitudinal motion, 8 PM
PM losses	Fig. 9	Fig. 10	Fig. 13	Fig. 14	Fig. 17
Damping Force	Fig. 11	-	-	Fig. 15	-
Damping coefficient	Fig. 12	-	Fig. 13	Fig. 16	Fig. 17

Table 3: Description of the cases considered for the results presented in Figures 9 to 17.

Figures 9 to 17 leads to the following comments:

- the losses, the force and the damping coefficient obtained during a transverse simulation do not depend on the stator longitudinal position since the losses curves of Figure 6 and 7 are quite similar;
- the use of 8 PM segments instead of 4 permits to reduce the losses with a factor of around 30 [%], but, as a consequence, the damping factor is quite low;
- for the longitudinal movement, Equations 21 and 22 are confirmed.

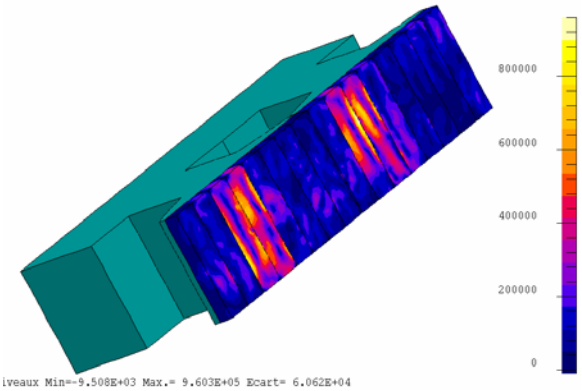

Figure 7: Color shaded of eddy current density.
Longitudinal simulation – 4 PM segments

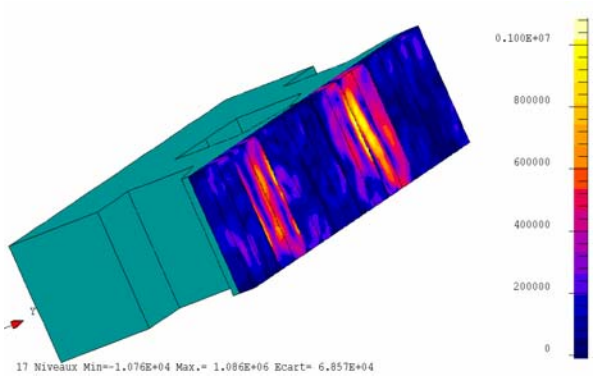

Figure 8: Color shaded of eddy currents.
Longitudinal simulation – 8 PM segments

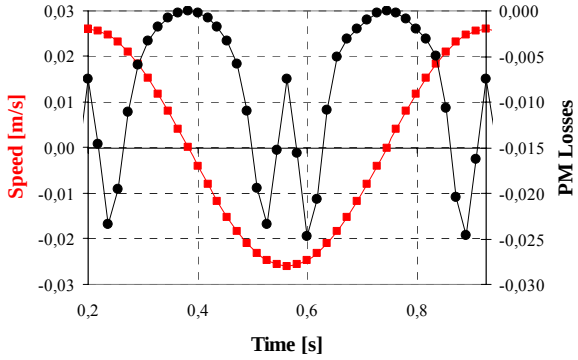

Figure 9: Vehicle PM losses versus time.
Transverse simulation – 4 PM segments – axis d

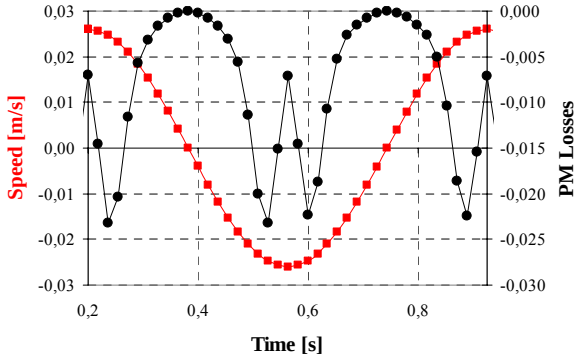

Figure 10: Vehicle PM losses versus time.
Transverse simulation – 4 PM segments – axis q

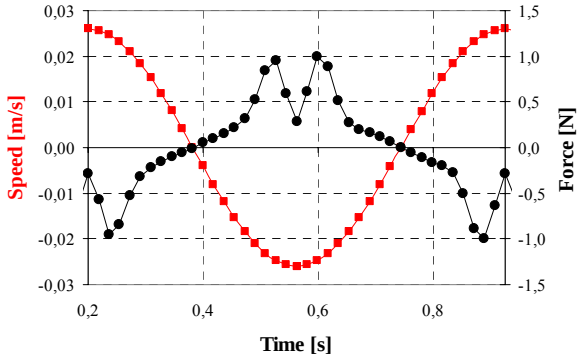

Figure 11: Vehicle damping force versus time.
Transverse simulation – 4 PM segments – axis d

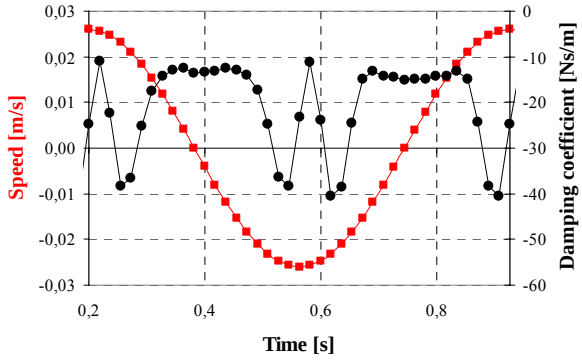

Figure 12: Vehicle damping coefficient versus time.
Transverse simulation – 4 PM segments – axis d

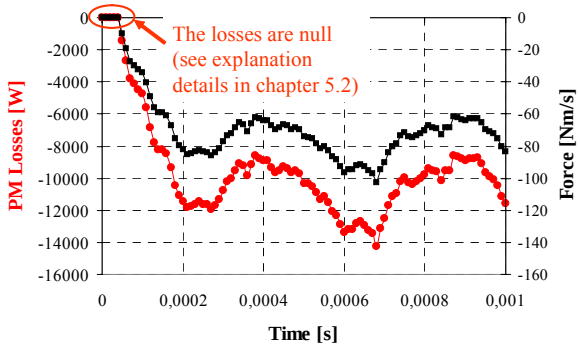

Figure 13: Vehicle PM losses and damping force versus time.
Longitudinal simulation – 4 PM segments

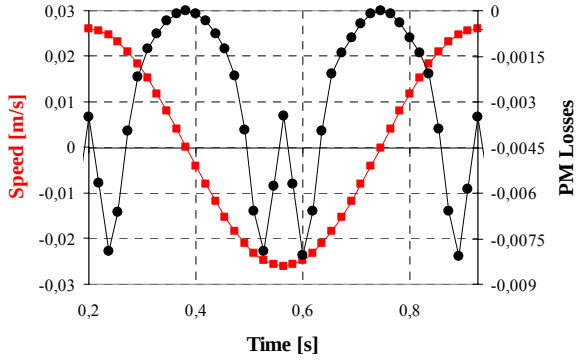

Figure 14: Vehicle PM losses versus time.
Transverse simulation – 8 PM segments – axis d

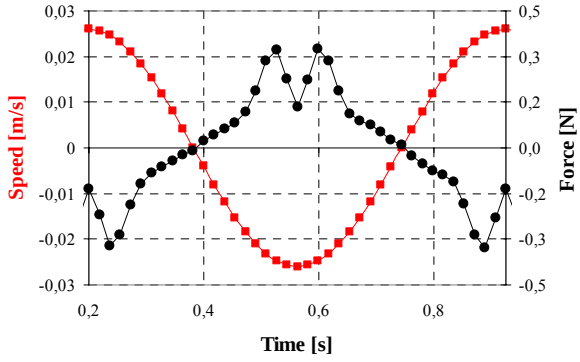

Figure 15: Vehicle damping force versus time.
Transverse simulation – 8 PM segments – axis d

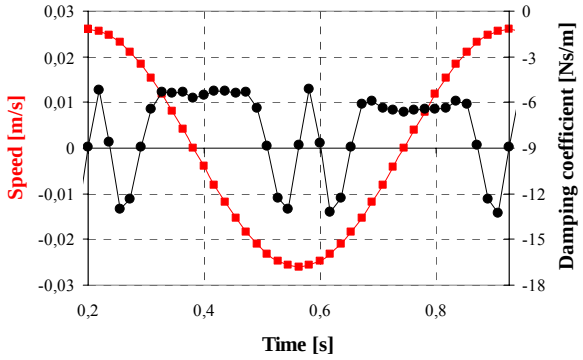

Figure 16: Vehicle damping coefficient versus time.
Transverse simulation – 8 PM segments – axis d

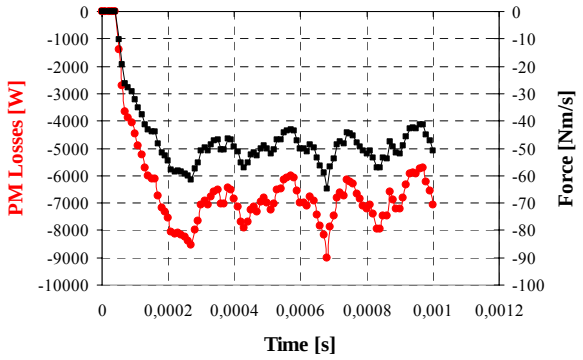

Figure 17: Vehicle PM losses and damping force versus time.
Longitudinal simulation – 8 PM segments

6. Dynamic Simulation Results

A first dynamic analysis has been carried out to evaluate the capability of the electromagnetic transverse damping to contribute to the lateral stabilization of the complete vehicle. A simulation is carried out without the second-level suspension shown in Figure 5 (m_{pr} and m_{se} are rigidly coupled), the simulation is based on Equations 13 to19 without the first member of Equation 20. Based on the results obtained in [5], the case of Table 2 is considered. The stiffness value of each mechanical spring is 3 [MN/m]. Considering a total vehicle mass of $8 \cdot 10^4$ [kg], the eigen frequency of the system is $\omega_0 = 8.66$ [rad/s], corresponding to a period of 0.725 [s] for the natural system oscillation. At a vehicle speed of 139 [m/s], this corresponds to 100.8 [m] critical guide way wave length ($2 \cdot D_{track}$). On the basis of the present results regarding the damping, a value of 11.6 [Ns/m] has been considered for each dash-pot of the mechanical system. The damping coefficient λ_{sys} and the damping factor η_{sys} [8] for the global system are defined by:

$$\lambda_{sys} \equiv \frac{k_{loss_{zr}} + k_{loss_{zl}}}{2 \cdot m_{vehicle}} = 14.5 \cdot 10^{-5} \quad [1/s] \qquad (31)$$

$$\eta_{sys} \equiv \frac{\lambda_{sys}}{\omega_0} = 1.67 \cdot 10^{-5} << 1 \quad [-] \qquad (32)$$

The damping factor allows for determining the behavior of the dynamical system. In this case, it is much smaller than one, the damping is therefore sub-critical, leading to significant oscillations, as shown on Figure 18.

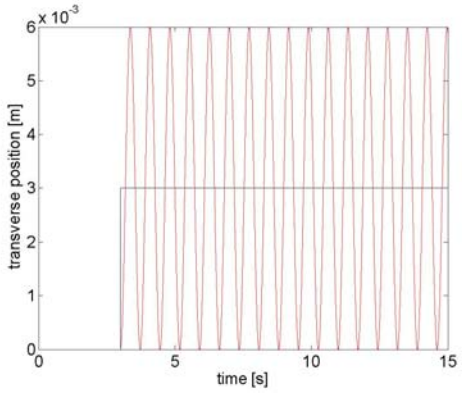

Figure 18: Oscillations (in red) of the system due to an increment step of 3 [mm] (in black) on both side of the guide way (here: z_s=z_w). The electromagnetic damping alone is obviously negligible.

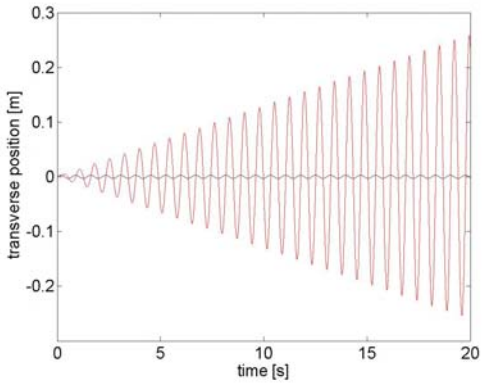

Figure 19: Oscillations (here again: z_s=z_w, in red) of the vehicle due to an harmonic geometry of 3 [mm] of amplitude (z_t in black) on both side of the guide way. The eigen frequency of the track geometry is equal to the eigen frequency of the system.

Another important aspect is the behavior of the system has it follows a harmonic guide way deflection as described by Equation 14. Figure 19 shows this behavior for the same dynamical system. The transient phase presented on Figure 19 tends to stabilize with time if damping exists. The "steady" amplification factor for the peak values μ_{max} can be computed as follows [8]:

$$\mu_{max} \equiv \frac{z_{s_{max}}}{z_{t_{max}}} = \frac{1}{2 \cdot \eta_{sys} \sqrt{1 - \eta_{sys}^2}} = 2.99 \cdot 10^4 \ [-] \qquad (33)$$

As can be seen, the amplification factor is extremely high. Therefore, this preliminary analysis shows that it is necessary to take additional measures to limit the amplification factor and to increase the damping effects. The electromagnetic damping alone is not sufficient to limit movement amplitudes near the eigen frequencies.

6.1. Proposed Approaches

Considering mechanical solutions, two types of solutions can be considered:

- adding a dynamical system is proposed in [5]. However, practical contingencies limit the performance of this type of solution (in particular, the mass to create the additional dynamical system is limited);

- adding a second damping level to isolate the primary mass (Fig. 5), can also be considered. The behavior of the magnetic way is still strongly sub-critical. But its eigen frequency is increased, which is favorable and the damping inside the vehicle is considerable increased. Figure 20 shows typical results for this solution.

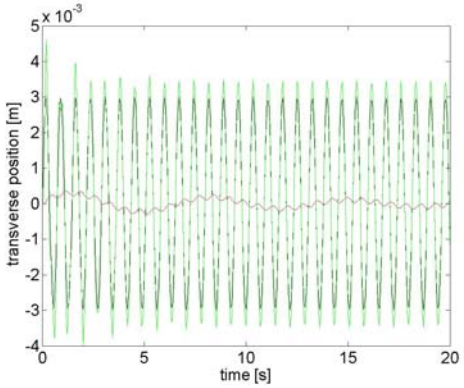

Figure 20: System positions: vehicle (z_s, in red) position due to the profile track of Table 2; amplitude on both sides of the guide way (z_{tr} in black) and position of the magnetic way (z_w, in green).
- mechanical spring coefficient: $5.9 \cdot 10^4$ [N/m];
- mechanical damping coefficient: 10100 [Ns/m];
- PM damping coefficients: 11.6 [Ns/m];
- primary mass: 68 [ton], secondary mass: 12 [ton].

Another approach is to integrate an **active electromechanical system**. It has the advantage of offering a high quality of comfort, since an active system can handle any kind of perturbations from track profile, track dynamics or aerodynamics. It has the disadvantage to add equipment on board of the vehicle.

The vehicle speed has a major effect on the dynamic behavior presented in this paper. Reducing the speed decreases the critical guide way length which reduces the track irregularities amplitude, as well as the transverse accelerations. This leads to a more favorable situation regarding damping, particularly if two damping levels are considered as illustrated on Figure 5.

7. Conclusions

- The mechanical and the electromechanical damping effects, characterized by the factors k_{pr_d} , $k_{loss_{PM}}$, are fully analyzed in the final paper. The factor k_{loss}, is a function of the speed and of the lateral eccentricities.
- Both mechanical damping using a secondary mass system and the damping due to the iron losses of the magnetic way are investigated. *The electromagnetic damping is not sufficient to handle dynamic effects associated with perturbations close to eigen frequencies, due to the very low damping factor* η_{sys} .
- As pointed out in [5], the primary static electromagnetic forces can match the specified guidance forces specifications. This paper demonstrates that the dynamics of the system needs to be controlled through an active electromechanical or a mechanical (preferably active) additional system.
- The complete method should involve the 3D FEM simulations with both motions in two independent axes and simultaneously the resolution of the dynamic equations of the system. Due to the actual limitations of 3D FEM software, this was not possible in this paper.

8. List of Symbols

D	track: half period of alignment	[m]
Fz	force (z component)	[N]
a	acceleration	[m/s^2]
d	track deflection	[m]
g	earth acceleration	[m/s^2]
k	force constant	[N/m]
kz	force constant (guidance force)	[Ns^2/m^2]
k_{loss}	force constant (guidance force)	[N/m2]
m	mass	[kg]
t	time	[s]
v	speed	
x	coordinate	[m]
y	coordinate	[m]
z	coordinate	[m]
β_0	shift between left tand right track profiles	[m]
δ	air gap	[m]
ω	pulsation	[1/s]

Indexes

PM	permanent magnet
l	left
pr	primary
r	right
t	track
s	stator
se	secondary
w	magnetic way

References

[1] A. Cassat, M. Jufer, "*MAGLEV Projects Technology Aspects and Choices*", IEEE Transactions on Applied Superconductivity, Vol. 12, Issue 1, March 2002, pp: 915-925.

[2] A. Cassat, C. Espanet, "*SWISSMETRO: Combined Propulsion with Levitation and Guidance*", MAGLEV 2004, October 26-28, 2004, Shanghai, China, Proceedings, pp 747-758, vol. II.

[3] A. Cassat, C. Espanet, V. Bourquin, P. Hagmann, M. Jufer, "*SWISSMETRO - Polarized Linear Motor Combined With Levitation Actuators*", LDIA 2005, September 25-28, 2005, pp 247-250, Awaji Yumebutai, Hyogo, Japan and also

[4] Reference [3] is also in IEEJ Trans. IA, VOL 126, No. 10, pp 1286-1292, 2006.

[5] A. Cassat, C. Espanet, V. Bourquin, M. Jufer, "*Passive Guidance Forces of Polarized Linear Motors Combined with Levitation Actuators Working in Partial Vacuum – Application to Swissmetro*", MAGLEV 2006, September 13-15, 2006, Dresden, Germany, Vol. I, pp 351-362.

[6] C. Zhao, W. Zhai, K. Wang, "*Dynamic Responses of the Low-speed Maglev Vehicle on the Curved Guideway*", MAGLEV 2004, October 26-28, 2004, Shanghai, China, Proceedings, pp 559-566, vol. II.

[7] W. Zhai, C. Zhao, C. Cai, "*Dynamic Simulation of the EMS Maglev Vehicle-Guideway-Controller Coupling System*", MAGLEV 2004, October 26-28, 2004, Shanghai, China, Proceedings, pp 567-574, vol. II.

[8] M. Del Pedro, P. Pahud: "*Mécanique vibratoire: systèmes discrets linéaires*", Presses Polytechniques Romandes, Lausanne, 1989.